Tin-Assisted Synthesis of ϵ-Ga_2O_3 by Molecular Beam Epitaxy

M. Kracht,[1,*] A. Karg,[1,3] J. Schörmann,[1] M. Weinhold,[1] D. Zink,[1] F. Michel,[1] M. Rohnke,[2] M. Schowalter,[3] B. Gerken,[3] A. Rosenauer,[3] P. J. Klar,[1] J. Janek,[2] and M. Eickhoff[1,3]

[1]*I. Physikalisches Institut, Justus-Liebig-Universität Gießen, Heinrich-Buff-Ring 16, 35392 Gießen, Germany*

[2]*Physikalisch-Chemisches Institut, Justus-Liebig-Universität Gießen, Heinrich-Buff-Ring 17, 35392 Gießen, Germany*

[3]*Institut für Festkörperphysik, Universität Bremen, Otto-Hahn-Allee 1, 28359 Bremen, Germany*

(Received 12 June 2017; revised manuscript received 25 August 2017; published 3 November 2017)

The synthesis of ϵ-Ga_2O_3 and β-Ga_2O_3 by plasma-assisted molecular beam epitaxy on $(001)Al_2O_3$ substrates is studied. The growth window of β-Ga_2O_3 in the Ga-rich regime, usually limited by the formation of volatile gallium suboxide, is expanded due to the presence of tin during the growth process, which stabilizes the formation of gallium oxides. X-ray diffraction, transmission electron microscopy, time-of-flight secondary-ion mass spectrometry, Raman spectroscopy, and atomic force microscopy are used to analyze the influence of tin on the layer formation. We demonstrate that it allows the synthesis of phase-pure ϵ-Ga_2O_3. A growth model based on the oxidation of gallium suboxide by reduction of an intermediate sacrificial tin oxide is suggested.

DOI: 10.1103/PhysRevApplied.8.054002

I. INTRODUCTION

Gallium oxides in general and the thermodynamically stable β-Ga_2O_3 in particular draw increasingly more attention due to their promising material properties. The large band gap around 5 eV enables the application as transparent conducting oxide, while the high breakdown field, which leads to a higher Baliga figure of merit compared to materials like SiC or GaN, favors the application in high-power electronic devices [1]. Gallium oxide can crystallize in at least five different polymorphs [2]. Recently, thin films of the thermodynamically stable β phase are grown by different deposition techniques like chemical vapor deposition (CVD) [3], pulsed-laser deposition (PLD) [4], and molecular beam epitaxy [5] and have intensely been studied. The growth window was investigated in detail by Vogt and Bierwagen, who found that, in metal-rich conditions, etching due to the formation and subsequent evaporation of volatile gallium suboxide (Ga_2O) occurs [6,7] and results in an attenuation of crystal growth.

While many material properties of the different polymorphs, such as the size of the optical band gap with values around 5 eV, are comparable [8], ϵ-Ga_2O_3 features one specific characteristic: Theoretical studies from Maccioni and Fiorentini predict a high spontaneous polarization along the $\langle 001 \rangle$ direction, principally allowing the realization of polarization-induced two-dimensional electron gases with high sheet carrier densities up to 1.6×10^{14} cm^{-2} in heterostructures with other materials such as GaN [9].

In Ref. [10], it was reported that ϵ-Ga_2O_3 possesses a hexagonal crystal structure (space group $P6_3mc$), facilitating heteroepitaxial growth on substrates like GaN, AlN, ZnO, or c-plane sapphire. By contrast, a closely related orthorhombic crystal structure with the space group $Pna2_1$ was suggested in Refs. [11,12].

Thin films of the metastable ϵ-Ga_2O_3 phase have rarely been synthesized. Different authors assigned the growth temperature as the most important parameter to obtain phase-pure ϵ-Ga_2O_3. Using CVD, Boschi *et al.* observed the formation of ϵ-Ga_2O_3 only at intermediate temperatures of about 650 °C, while, at lower or higher temperatures, amorphous or β-Ga_2O_3 thin films were formed [13]. Oshima *et al.* reported the stabilization of ϵ-Ga_2O_3 on β-Ga_2O_3 substrates by CVD at a growth temperature of 550 °C, whereas growth at 1050 °C led to β-Ga_2O_3 [14]. Orita *et al.* observed a phase change from β-Ga_2O_3 to ϵ-Ga_2O_3 at temperatures above 410 °C for Sn-doped layers grown by PLD [4]. Zhao *et al.* presented the growth of tin containing ϵ-Ga_2O_3 at substrate temperatures above 750 °C [15].

In this work, ϵ-Ga_2O_3 layers are grown by plasma-assisted molecular beam epitaxy (PAMBE) on c-plane sapphire. Besides the low concentration of nonintentional impurities in the resulting layers, this growth technique basically allows the precise control of doping and the realization of heterostructures with sharp interfaces. We demonstrate that the presence of tin expands the growth window of Ga_2O_3 to the metal-rich regime and ϵ-Ga_2O_3 can be stabilized in these growth conditions. In addition to a detailed structural characterization of the tin-induced transition from β-Ga_2O_3 to ϵ-Ga_2O_3, we suggest a model for

*Max.E.Kracht@materialwiss.uni-giessen.de

the observed phenomena, taking the oxidation of volatile gallium suboxide by reduction of an intermediate sacrificial tin oxide on the substrate surface into account.

II. EXPERIMENT

Ga_2O_3 thin films are grown by PAMBE on (001)-oriented sapphire substrates in a Riber Compact 12 system. A 1.2-μm molybdenum backside metallization is used to facilitate radiative heating. Prior to growth, the substrates are cleaned in acetone in an ultrasonic bath and afterwards in isopropanol, followed by a 10-min O_2 plasma treatment at 700 °C in the growth chamber. The growth temperature is set to 700 °C. Gallium and tin are provided by effusion cells. As a measure for the metal fluxes, a pressure gauge at the sample position is used to determine the beam equivalent pressure (BEP). An Oxford Applied Research (HD 25) plasma source with an ion deflection unit is used for oxygen supply. If not specified otherwise, the plasma power during growth is kept constant at 150 W and the O_2 flow is set to 0.5 sccm. Three different sample series are prepared: In series A, the gallium BEP (BEP_{Ga}) is varied from 2.1×10^{-8} to 2.74×10^{-7} mbar, and no Sn is supplied ($BEP_{Sn} = 0$). In series B, the BEP_{Ga} is varied from 2.1×10^{-8} to 4.2×10^{-7} mbar with a constant BEP_{Sn} of 1.17×10^{-11} mbar, while, in series C, the BEP_{Ga} is kept at 1.77×10^{-7} mbar, and the BEP_{Sn} is varied from 0 to 1.46×10^{-9} mbar. For a BEP_{Sn} below 5×10^{-8} mbar, the actual values are obtained by extrapolating the measured BEP_{Sn} values above 5×10^{-8} mbar to lower cell temperatures, assuming an Arrhenius behavior. The structural properties of the samples are characterized by high-resolution x-ray diffraction (HRXRD) using a PANalytical X'pert Pro MRD diffractometer and by atomic force microscopy (AFM) using a SmartSPM 1000 (AIST-NT). The film thickness is determined from optical reflection.

To evaluate the incorporation of tin during growth time-of-flight secondary-ion mass spectrometry (TOF-SIMS) measurements are performed using an ION-TOF 5-100 spectrometer (ION-TOF GmbH, Muenster, Germany). In these measurements, 1-keV O_2^+ ions are used for sputtering ($I = 347$ nA, sputter area $= 200 \times 200$ μm^2), while 25 keV Bi^+ ions are used as primary ions ($I = 1.84$ pA, analysis area $= 100 \times 100$ μm^2). The primary ion gun is operated in high-current bunched mode and the achieved mass resolution is $m/\Delta m > 11\,100$ for $^{71}Ga^-$ ($m/z = 70.93$). For tin, the three most abundant isotopes, $^{120}Sn^+$, $^{118}Sn^+$, and $^{116}Sn^+$, and, for gallium, the signals of $^{69}Ga^+$ and $^{71}Ga^+$ are evaluated. The absolute tin concentration is estimated using a tin-doped ϵ-Ga_2O_3 wafer with a carrier concentration of 2.4×10^{18} cm^{-3} supplied by Tamura Corp. as a reference, assuming similar matrix characteristics of ϵ-Ga_2O_3 and β-Ga_2O_3 and a 100% doping efficiency in β-Ga_2O_3.

Transmission-electron-microscopy (TEM) specimens are prepared in a focused-ion-beam scanning electron microscope (FIB-SEM) Nova fabricated by FEI, which is equipped with a Kleindiek manipulator for transfer of the lamella from the sample to a Cu support grid. TEM characterization is carried out in an FEI Titan 80-300 ST equipped with a corrector for spherical aberration of the objective lens.

Raman spectra at room temperature are obtained using a Renishaw microscope system operating in backscattering geometry. Linearly polarized laser light of a 532- or 488-nm wavelength is used for excitation. No polarizers are used for detection. The measurements are performed in confocal mode in order to restrict the scattering volume in depth.

III. RESULTS AND DISCUSSION

A. Expansion of the Ga_2O_3 growth window with tin

In Fig. 1, the growth rates of Ga_2O_3 as a function of BEP_{Ga} are shown for series A (the black squares) and series B (the red triangles). For both series, an initial increase with increasing Ga flux is observed in the Ga-limited oxygen-rich growth regime. For series A ($BEP_{Sn} = 0$), the growth rate reaches a maximum at the transition to metal-rich conditions around $BEP_{Ga} = 5 \times 10^{-8}$ mbar before it decreases to zero for a higher BEP_{Ga}. According to Refs. [6,7], Ga_2O is formed at the surface and subsequently evaporates in this regime. As metallic gallium can also react with already-deposited Ga_2O_3 to form Ga_2O, this suboxide formation leads to etching of the film. As is also shown in Fig. 1, the presence of tin during growth of series B results in a significant increase of the maximum growth rate by a

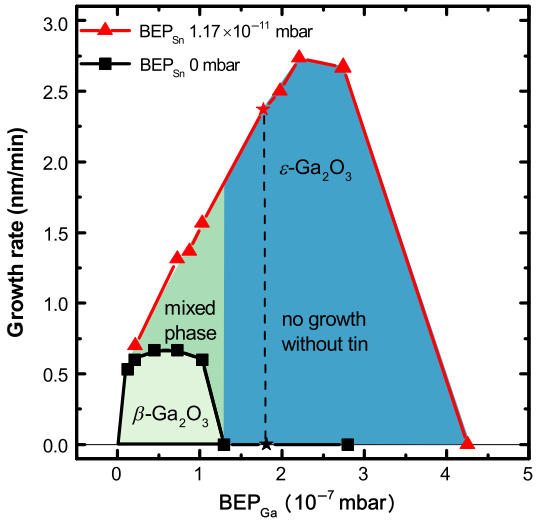

FIG. 1. Comparison of the growth rates of series B and A (with and without tin) as a function of BEP_{Ga}. An attenuation of etching and an expansion of the growth window with the presence of tin are observed.

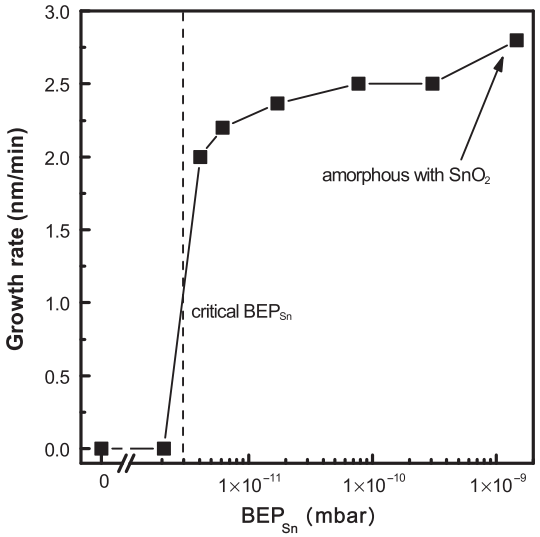

FIG. 2. Growth rate at a BEP_{Ga} of 1.77×10^{-7} mbar as a function of BEP_{Sn} (series C). Only above a critical BEP_{Sn} of 4×10^{-12} mbar growth is observed.

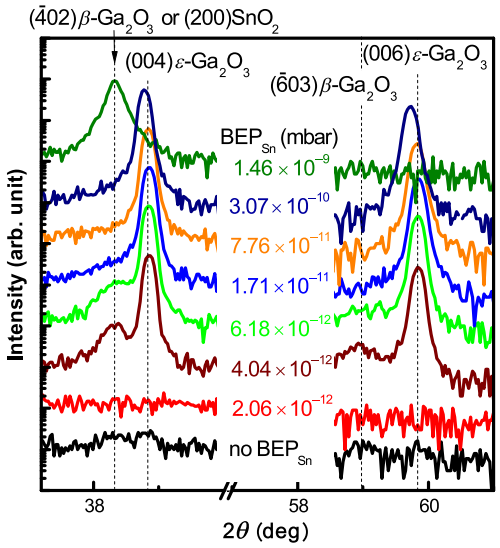

FIG. 3. ω-2θ scans of the samples grown at a BEP_{Ga} of 1.77×10^{-7} mbar and at different BEP_{Sn} values (series C). The presence of tin stabilizes ϵ-Ga_2O_3.

factor of 5 and in a shift of the maximum to a higher BEP_{Ga} value of 2.1×10^{-7} mbar, i.e., tin suppresses etching due to suboxide formation.

This result is confirmed by the data displayed in Fig. 2, which shows the evolution of the growth rate in the gallium-rich growth regime for a BEP_{Ga} of 1.77×10^{-7} mbar as a function of the applied BEP_{Sn} (series C, with data points marked with star symbols along the dashed line in Fig. 1). Without the presence of tin, the formation of volatile Ga_2O prohibits the growth of Ga_2O_3. Above a critical tin flux between 2×10^{-12} and 4×10^{-12} mbar, etching is attenuated and a growth rate of 2 nm/min is observed. When increasing BEP_{Sn} over 2 orders of magnitude, the growth rate shows only a slight further increase. The highest growth rate of 2.8 nm/min is observed for the sample with BEP_{Sn} of 1.46×10^{-9} mbar.

B. Influence of tin on phase formation

The threshold behavior indicated above is also confirmed by the results of the XRD analysis, presented by the ω-2θ scans measured in Bragg-Brentano geometry for the samples of series C (discussed in Fig. 2) in Fig. 3. The two samples with a BEP_{Sn} below the threshold show only reflexes from the sapphire substrate. The two samples with a BEP_{Sn} of 4.04×10^{-12} mbar and 6.18×10^{-12} mbar show additional reflexes at $2\theta = 38.3°$ and 38.8°, which can be assigned to $(-402)\beta$-Ga_2O_3 and $(004)\epsilon$-Ga_2O_3, respectively, indicating the coexistence of both phases in this regime. Additionally, higher orders of these reflexes, $(-603)\beta$-Ga_2O_3 and $(006)\epsilon$-Ga_2O_3, are observed at $2\theta = 59°$ and 59.8°. For samples grown with a higher BEP_{Sn}, the β-Ga_2O_3 reflexes disappear and the formation of phase-pure ϵ-Ga_2O_3 is observed. Only for the sample with the highest BEP_{Sn} of 1.46×10^{-9} mbar are the ϵ-Ga_2O_3 reflexes no longer visible, and a single reflex without any higher-order reflexes appears at $2\theta = 38.3°$ and can be assigned to $(200)SnO_2$. Since the total amount of deposited Sn would not be sufficient to grow a pure SnO_2 layer thicker than 40 nm and the overall film thickness is above 350 nm, we assume the formation of an amorphous Ga_2O_3 layer with SnO_2 inclusions. Hence, the presence of tin on the surface induces the phase formation of ϵ-Ga_2O_3. It should be noted that the formation of phase-pure ϵ-Ga_2O_3 is promoted only for a medium BEP_{Sn} on the order of 10^{-11} mbar. A lower tin flux allows for the simultaneous growth of β-Ga_2O_3, and significantly higher flux leads to the formation of an amorphous film. The influence of tin on the structural properties of the ϵ-Ga_2O_3 films determined by XRD rocking-curve measurements is further examined in the Supplemental Material [16].

The XRD ω-2θ scans of the samples of series B, displayed in Fig. 4, show that the transition from β-Ga_2O_3 to ϵ-Ga_2O_3 at a given tin flux also depends on the gallium-to-oxygen ratio during growth. While the samples with $BEP_{Ga} > 1.77 \times 10^{-7}$ mbar exhibit only the $(004)\epsilon$-Ga_2O_3 reflex, the diffraction patterns of samples grown with lower BEP_{Ga} values show an additional shoulder at lower angles that corresponds to the $(-402)\beta$-Ga_2O_3 reflex. For the lowest BEP_{Ga} values, only this reflex is detectable. This dependence of the phase transition on the surface stoichiometry is independently confirmed by a variation of the plasma power, i.e., the amount of activated oxygen (also Fig. 4). In this experiment, a higher plasma power of 350 W is chosen, while BEP_{Ga} and BEP_{Sn} are kept constant. This growth conditions resulted in the formation of a β-Ga_2O_3/ϵ-Ga_2O_3 mixed-phase sample dominated by β-Ga_2O_3. This result is

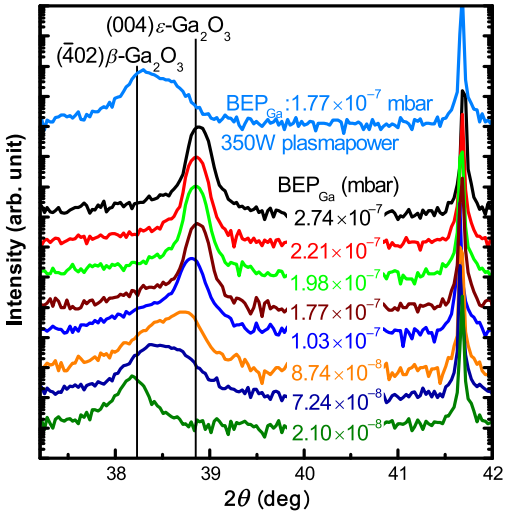

FIG. 4. The ω-2θ scans of samples of series B and an additional sample with a higher plasma power (350 W) are shown. Oxygen-rich conditions lead to the formation of β-Ga_2O_3, whereas gallium-rich conditions lead to the formation of ϵ-Ga_2O_3. This holds for both the variation of BEP_{Ga} and the oxygen plasma power, as shown in the top curve.

in contrast to the phase-pure ϵ-Ga_2O_3 sample obtained with a plasma power of 150 W.

The role of tin in the phase stabilization process is further examined by analyzing its incorporation using TOF SIMS. In Fig. 5, the depth profiles for tin and gallium for the samples of series C are shown. The constant Sn and Ga signals in the layer region indicate a homogeneous incorporation of these elements in the Ga_2O_3 layer. The Sn concentration increases linearly to a value of 6% with the applied BEP_{Sn} (the inset in Fig. 5). An exception to this behavior is the sample grown at the highest BEP_{Sn} value of

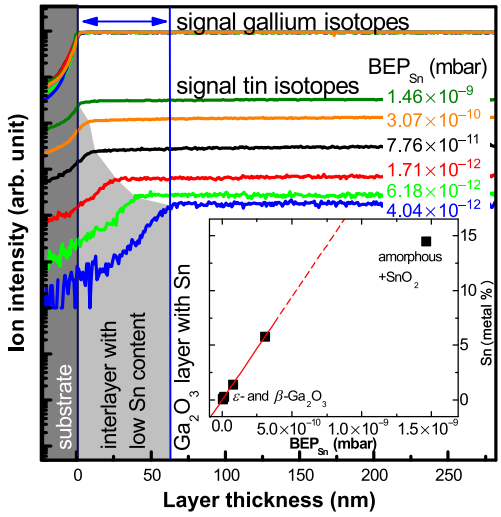

FIG. 5. Results of the TOF-SIMS analysis for samples with different BEP_{Sn} (series C). (Inset) Linear dependence of the tin content on the BEP_{Sn}.

1.46×10^{-9} mbar, which shows a tin concentration that is a factor of 2 lower than the corresponding value extrapolated from the other samples. We attribute this behavior to a change of the matrix material, as this sample is amorphous with SnO_2 inclusions (shown above). For all samples, the strong decrease of the gallium signal coincides with the increase of the aluminum signal from the sapphire (not shown), indicating the transition to the substrate.

In the depth profiles in Fig. 5, a decrease of the tin signal already at a larger distance from the interface can be observed, thus defining a transition layer with a continuously decreasing tin concentration. The thickness of this transition layer decreases with an increasing BEP_{Sn}. However, the exact incorporation mechanism of Sn in Ga_2O_3 is not clear. Analysis by x-ray photoelectron spectroscopy (see the Supplemental Material [16]) suggests that the oxidation state of incorporated tin is 4^+. Furthermore, except for the sample with the highest BEP_{Sn}, there is no evidence for the existence of crystalline SnO_x in the XRD data. Therefore, we assume that tin is incorporated into the Ga_2O_3 crystallites, on either a substitutional or an interstitial lattice site.

In Figs. 6(b) and 6(c), TEM images of a pure ϵ-Ga_2O_3 and a mixed β-Ga_2O_3/ϵ-Ga_2O_3 sample (from series C with a BEP_{Sn} of 7.76×10^{-11} and 6.18×10^{-12} mbar, respectively) are shown; Fig. 6(a) displays the micrograph of a pure β-Ga_2O_3 sample for reference. In contrast to the β-Ga_2O_3 sample, the pure ϵ-Ga_2O_3 sample exhibits

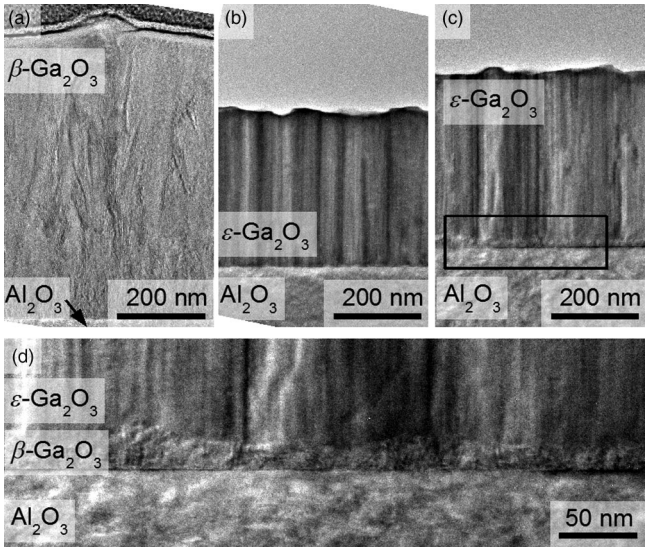

FIG. 6. Bright-field TEM images of (a) a pure β-Ga_2O_3, (b) a pure ϵ-Ga_2O_3, and (c) a mixed β-Ga_2O_3/ϵ-Ga_2O_3 sample. In contrast to the image of the pure β-Ga_2O_3 sample, the image of the pure ϵ-Ga_2O_3 sample shows columnar contrasts starting directly at the interface to the substrate. The image of the mixed sample also shows columnar contrasts but exhibits an intermediate layer at the interface to the substrate. (d) A magnified image [the rectangle in (c)] of the mixed β-Ga_2O_3/ϵ-Ga_2O_3 sample at the interface.

columnar contrasts, indicating a columnar growth of the material. Electron diffraction patterns (not shown here) of both layers confirm the crystal structure of the samples determined from the XRD measurements shown earlier. The image of the mixed β-Ga_2O_3/ϵ-Ga_2O_3 sample in Figs. 6(c) and 6(d) also reveals a columnar contrast similar to the contrast seen in the pure ϵ-Ga_2O_3 sample. However, the columnar contrast here does not start directly at the interface to the substrate, but an intermediate layer is observed [see Fig. 6(d) for a magnified view of the interface region]. The thickness of this intermediate layer varies, evidencing a more 3D nature. This interlayer also becomes apparent from the diffraction pattern of this region, where, basically, a diffraction pattern of β-Ga_2O_3 is observed, with additional spots corresponding to ϵ-Ga_2O_3.

A comparison of the XRD results (Fig. 3), the TOF-SIMS profiles (Fig. 5) and the TEM observations (Fig. 6) proves the existence of a β-Ga_2O_3 transition layer with a lower concentration of incorporated tin close to the sapphire substrate, followed by a region of ϵ-Ga_2O_3 with a higher concentration of incorporated tin. The thickness of the transition layer decreases with an increasing BEP_{Sn}. Hence, it can be concluded that the incorporation of a critical concentration of tin in gallium-rich conditions initiates the transition from β-Ga_2O_3 to ϵ-Ga_2O_3 growth.

C. Structural properties of ϵ-Ga_2O_3

The surface morphology of the ϵ-Ga_2O_3 samples is characterized by the presence of small crystallites with diameters of around 50 nm that agglomerate and form larger clusters with sizes of 250 nm, resulting in a rms roughness of 4 to 5 nm, revealed by atomic force microscopy (Fig. 7). By comparison, a phase-pure β-Ga_2O_3 surface exhibits crystallites with a size of around 100 nm and a rms surface roughness of 3.8 nm.

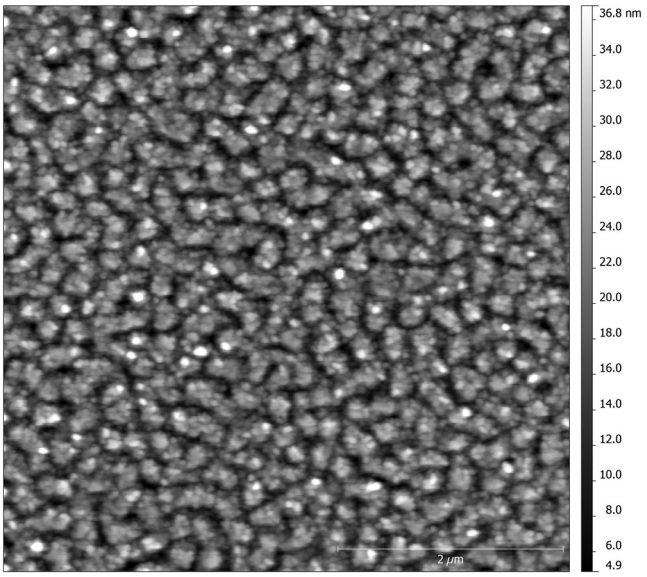

FIG. 7. The AFM micrograph of a ϵ-Ga_2O_3 sample shows the surface structure of approximately 50-nm-diameter crystallites.

As the 2θ values for the $(-402)\beta$-Ga_2O_3 reflex and the $(004)\epsilon$-Ga_2O_3 reflex in the HRXRD analysis shown in Figs. 3 and 4 differ only slightly, HRXRD analysis by ϕ scans is carried out to further identify the different phases of Ga_2O_3. Figure 8 shows ϕ scans of the phase-pure ϵ-Ga_2O_3 layer from series B grown with the highest growth rate on c-plane sapphire. The top curve (displayed in red) is measured at a 2θ value of 25.57° and a χ value of 57.6° and shows the threefold symmetry of the $(012)Al_2O_3$ reflex of the substrate. The second curve (in green) is measured with a 2θ value of 37.2° and a χ value of 74.8° and displays six reflexes with a distance of 60°. These reflexes can be assigned to the $(011)\epsilon$-Ga_2O_3 planes assuming a hexagonal lattice with the symmetry group $P6_3mc$, as described by Playford *et al.* [10], or the $(211)\epsilon$-Ga_2O_3 planes assuming an orthorhombic lattice with the symmetry group $Pna2_1$, as described by Yoshioka *et al.* [11]. To distinguish between these two closely related structures, another ϕ scan for a 2θ value of 33.05° and a χ value of 54.67° is performed. At this angle, only the (122) reflex of the orthorhombic lattice can be found, as the hexagonal lattice has no reflexes at this position. The result is shown at the bottom (the black line) of Fig. 8. There, the 12 peaks can be explained by three rotation domains of orthorhombic ϵ-Ga_2O_3, each contributing four reflexes, as indicated in the inset in Fig. 8. Hence, we conclude that, for the growth conditions applied here, ϵ-Ga_2O_3 in the orthorhombic $Pna2_1$ symmetry, as suggested by Yoshioka *et al.* [11], is formed. The in-plane

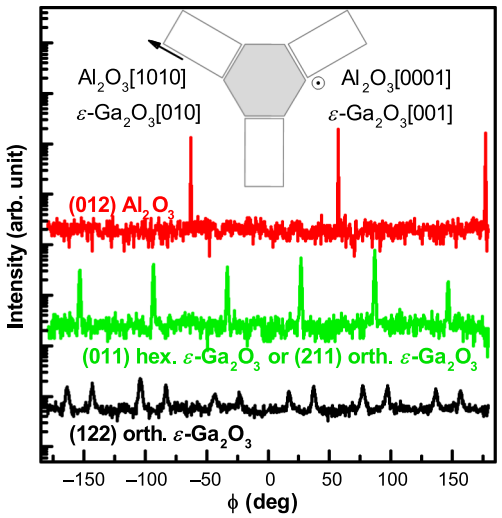

FIG. 8. ϕ scans of a ϵ-Ga_2O_3 sample performed for different sample orientations. The black line shows the ϕ scan for the (122) reflex of orthorhombic ϵ-Ga_2O_3. The red and green lines display the ϕ scan for the $(012)Al_2O_3$ and the (211) reflex of orthorhombic ϵ-Ga_2O_3, respectively. (Inset) Schematic of the relative in-plane orientation of the unit cells with three different rotation domains.

orientation of the layers is $[010]\epsilon\text{-}Ga_2O_3 \| [10.0]Al_2O_3$, with three domains rotated by 120° each.

The reported Raman spectra of α-, β-, and γ-Ga_2O_3 phases differ in the number of modes as well as in the respective mode frequencies [17–21]. Such differences compared to the other phases are also expected to hold for the ϵ phase. The optical transparency of the Ga_2O_3 films in the spectral range of the laser excitation and the resulting superposition with Raman signals from the sapphire substrate cause difficulties in obtaining spectra of Ga_2O_3 epitaxial films. Here, these detrimental effects are circumvented by performing Raman measurements in confocal mode on an epitaxial layer with a thickness of 1.13 μm, grown at a substrate temperature of 700 °C at BEP_{Ga} and BEP_{Sn} of 1.77×10^{-7} and 1.17×10^{-11} mbar, respectively, i.e., in the growth regime of phase-pure ϵ-Ga_2O_3, according to Fig. 1.

The spectra of the Ga_2O_3 thin film on sapphire and of a plain sapphire substrate are shown in Fig. 9. Although their comparison clearly indicates that the Raman spectrum of the thin film on sapphire is dominated by the Raman features of the sapphire substrate, additional weak Raman signals, which must originate from the Ga_2O_3 epitaxial film, can be observed and are indicated by vertical arrows in the difference spectrum shown in the lower panel of Fig. 9. The dotted, dotted-dashed, and dashed lines mark the positions of the Raman features of α-, β-, and γ-Ga_2O_3, respectively, and are taken from the literature [17,19,21].

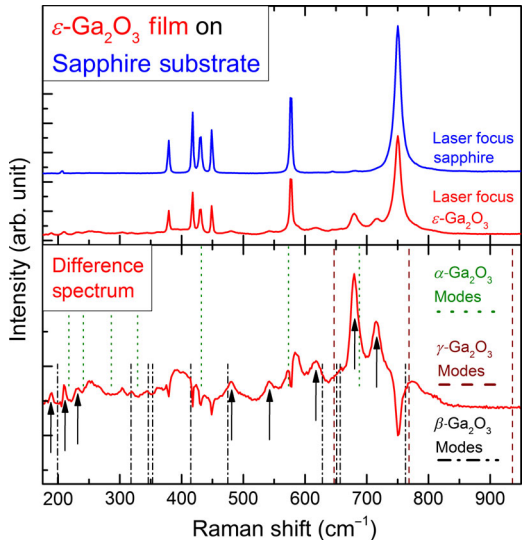

FIG. 9. (Top panel) Raman spectra of a sapphire substrate and a ϵ-Ga_2O_3 epitaxial thin film grown on a sapphire substrate. (Bottom panel) Difference spectrum revealing one-phonon Raman signals of ϵ-Ga_2O_3 (indicated by arrows). Dotted, dotted-dashed, and dashed lines correspond to the frequencies of the one-phonon Raman signals of α-, β-, and γ-Ga_2O_3, respectively, and are shown for comparison.

It is evident that the eight signals at 189, 211, 233, 481, 545, 616, 680, and 715 cm^{-1} cannot be assigned to a superposition of the spectra of the other Ga_2O_3 phases and, therefore, they are characteristic for the ϵ phase. A group theoretical analysis on the basis of an orthorhombic crystal structure (space group $Pna2_1$) based on the suggestions by Yoshioka *et al.* [11] yields 12 Raman-active modes with representations $3A_1 + 3A_2 + 3B_1 + 3B_2$ for the phonons in the center of the Brillouin zone. A corresponding analysis for the hexagonal structure (space group $P6_3mc$) proposed by Playford *et al.* [10] yields six Raman-active modes only, with representations $2A_1 + 2E_1 + 2E_2$.

All of the identified Raman signals lie in the range typical for the one-phonon Raman spectra of the other Ga_2O_3 phases. Therefore, it is likely that all of these signals correspond to one-phonon Raman scattering. As the number of signals observed is larger than 6 (the number of Raman active modes in the case of a hexagonal structure), these results are only in accordance with the predictions for the orthorhombic structure of ϵ-Ga_2O_3 and thus are in agreement with the XRD analysis.

Various reasons may be anticipated for the number of observed Raman features being less than 12: Additional signals might be present at Raman shifts below 150 cm^{-1}, which are not accessible in our measurements, or some of the Raman features, despite the subtraction of the sapphire features, cannot be detected in the range under study, or, due to selection rules, some Raman signals are not observable in the scattering geometry used.

D. Model for tin-assisted growth of ϵ-Ga_2O_3

According to Ref. [7], volatile gallium suboxide Ga_2O is formed and desorbs from the sample surface when metal-rich growth conditions are applied. Here, it was observed that the presence of tin on the surface attenuates the resulting etching process. We assign this finding to the fact that SnO_2 and SnO are formed in the presence of tin adatoms (see Fig. 10) which can react with Ga_2O, having been reduced to SnO or metallic Sn, while Ga_2O is oxidized to Ga_2O_3, according to the following reactions:

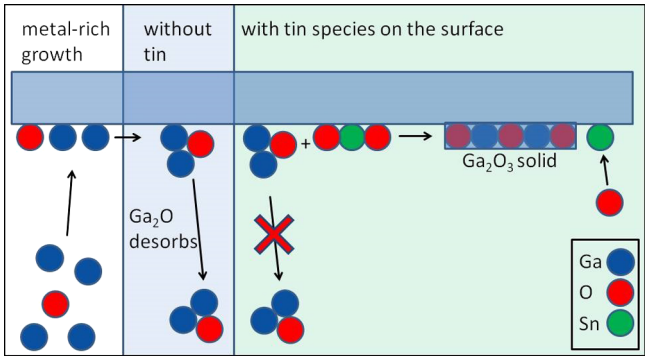

FIG. 10. Model for tin-assisted growth in metal-rich conditions.

$$Ga_2O + 2SnO_2 \leftrightharpoons Ga_2O_3 + 2SnO \quad \Delta G^0 = -93.7\,\mathrm{kJ/mol}$$
$$Ga_2O + 2SnO \leftrightharpoons Ga_2O_3 + 2Sn \quad \Delta G^0 = -117.7\,\mathrm{kJ/mol}$$
$$Ga_2O + SnO_2 \leftrightharpoons Ga_2O_3 + Sn \quad \Delta G^0 = -105.7\,\mathrm{kJ/mol}.$$

The standard Gibbs energies ΔG^0 are calculated from the standard enthalpy of formation and the standard entropy of formation values of the respective species [22,23]. The negative values for ΔG^0 indicate a high probability for these reactions on the surface. The reduced tin species might be reoxidized to SnO and SnO_2 that can further oxidize Ga_2O. We believe these intermediate tin species act as an intermediate oxygen trap that provides oxygen on the surface and attenuates the etching process.

E. Influence of tin on phase formation

We show above that tin-assisted growth not only expands the growth window to more gallium-rich conditions—it also promotes the formation of ϵ-Ga_2O_3. A possible reason for the latter effect is the ordering of atoms in the respective crystal structures: Comparing the coordination spheres for gallium lattice sites in β- and ϵ-Ga_2O_3, one finds that, in β-Ga_2O_3, half of the gallium atoms show a tetrahedral and the other half an octahedral coordination. By contrast, the ratio of tetrahedral to octahedral coordinated metal atoms is 1:3 in orthorhombic ϵ-Ga_2O_3. In a rutile SnO_2 crystal, the tin ions show an octahedral coordination with oxygen atoms, and hence the addition of tin to Ga_2O_3 might favor the octahedral positions. As the bond length in SnO_2 is larger than 2 Å, the latter effect is further enhanced by the influence of the metal-oxygen bond length, which is shorter in tetrahedral positions (< 1.9 Å) than in octahedral positions (> 1.9 Å) for all of the discussed Ga_2O_3 phases. Calculations by Varley *et al.* also reveal that the octahedral lattice site is preferred by tin atoms in Ga_2O_3 [24]. Therefore, additional tin might stabilize the phase with more octahedral lattice sites.

IV. CONCLUSION

In this paper, we demonstrate that the presence of tin during the growth of Ga_2O_3 on *c*-plane sapphire substrates by plasma-assisted molecular beam epitaxy leads to a drastic change of the growth characteristics. First, it leads to an expansion of the growth window to more gallium-rich conditions and causes a substantial increase of the achievable growth rate. We assign this observation to the formation of intermediate tin-oxide species that act as additional oxygen reservoirs on the growing surface, oxidizing volatile suboxides and thus stabilizing the growth of Ga_2O_3. Hence, the addition of adatoms that serve as intermediate oxygen reservoirs is a versatile technique to overcome growth limitations caused by the formation of volatile suboxides.

As a second effect, the presence of tin above a critical concentration, corresponding to a BEP_{Sn} of $\geq 10^{-11}$ mbar, in metal-rich growth conditions results in the formation of phase-pure orthorhombic ϵ-Ga_2O_3 on *c*-plane sapphire. For smaller tin concentrations, a ϵ-Ga_2O_3 transition layer is formed that decreases in thickness with an increasing BEP_{Sn}. The concentration of Sn in this intermediate layer is smaller than in the adjacent ϵ-Ga_2O_3 region and increases with thickness, the accumulation of tin on the surface could be identified as the origin of the phase transition as it promotes the formation of octahedral metal-oxygen bonds which are dominating in ϵ-Ga_2O_3. Hence, the addition of tin during growth presents a viable route for the synthesis of phase-pure ϵ-Ga_2O_3.

[1] Masataka Higashiwaki, Kohei Sasaki, Hisashi Murakami, Yoshinao Kumagai, Akinori Koukitu, Akito Kuramata, Takekazu Masui, and Shigenobu Yamakoshi, Recent progress in Ga_2O_3 power devices, Semicond. Sci. Technol. **31**, 034001 (2016).

[2] Rustum Roy, V. G. Hill, and E. F. Osborn, Polymorphism of Ga_2O_3 and the system Ga_2O_3-H_2O, J. Am. Chem. Soc. **74**, 719 (1952).

[3] Michele Baldini, Martin Albrecht, Andreas Fiedler, Klaus Irmscher, Detlef Klimm, Robert Schewski, and Günter Wagner, Semiconducting Sn-doped β-Ga_2O_3 homoepitaxial layers grown by metal organic vapour-phase epitaxy, J. Mater. Sci. **51**, 3650 (2016).

[4] Masahiro Orita, Hidenori Hiramatsu, Hiromichi Ohta, Masahiro Hirano, and Hideo Hosono, Preparation of highly conductive, deep ultraviolet transparent β-Ga_2O_3 thin film at low deposition temperatures, Thin Solid Films **411**, 134 (2002).

[5] Encarnacion G. Villora, Kiyoshi Shimamura, Kenji Kitamura, and Kazuo Aoki, Rf-plasma-assisted molecular-beam epitaxy of $\beta - Ga_2O_3$, Appl. Phys. Lett. **88**, 031105 (2006).

[6] Patrick Vogt and Oliver Bierwagen, The competing oxide and sub-oxide formation in metal-oxide molecular beam epitaxy, Appl. Phys. Lett. **106**, 081910 (2015).

[7] Patrick Vogt and Oliver Bierwagen, Reaction kinetics and growth window for plasma-assisted molecular beam epitaxy of Ga_2O_3: Incorporation of Ga vs. Ga_2O desorption, Appl. Phys. Lett. **108**, 072101 (2016).

[8] J. Furthmüller and F. Bechstedt, Quasiparticle bands and spectra of Ga_2O_3 polymorphs, Phys. Rev. B **93**, 115204 (2016).

[9] Maria Barbara Maccioni and Vincenzo Fiorentini, Phase diagram and polarization of stable phases of $(Ga_{1-x}In_x)_2O_3$, Appl. Phys. Express **9**, 041102 (2016).

[10] Helen Y. Playford, Alex C. Hannon, Emma R. Barney, and Richard I. Walton, Structures of uncharacterised polymorphs of gallium oxide from total neutron diffraction, Chem. Eur. J. **19**, 2803 (2013).

[11] S. Yoshioka, H. Hayashi, A. Kuwabara, F. Oba, K. Matsunaga, and I. Tanaka, Structures and energetics of Ga_2O_3 polymorphs, J. Phys. Condens. Matter **19**, 346211 (2007).

[12] Ildiko Cora, Francesco Mezzadri, Francesco Boschi, Matteo Bosi, Maria Caplovicova, Gianluca Calestani, Istvan Dodony, Bela Pecz, and Roberto Fornari, The real structure of ϵ-Ga_2O_3 and its relation to κ-phase, CrystEngComm **19**, 1509 (2017).

[13] F. Boschi, M. Bosi, T. Berzina, E. Buffagni, C. Ferrari, and R. Fornari, Hetero-epitaxy of β-Ga_2O_3 layers by MOCVD and ALD, J. Cryst. Growth **443**, 25 (2016).

[14] Yuichi Oshima, Encarnación G Víllora, Yoshitaka Matsushita, Satoshi Yamamoto, and Kiyoshi Shimamura, Epitaxial growth of phase-pure ε-Ga_2O_3 by halide vapor phase epitaxy, J. Appl. Phys. **118**, 085301 (2015).

[15] Xiaolong Zhao, Yusong Zhi, Wei Cui, Daoyou Guo, Zhenping Wu, Peigang Li, Linghong Li, and Weihua Tang, Characterization of hexagonal $\epsilon - Ga_{1.8}Sn_{0.2}O_3$ thin films for solar-blind ultraviolet applications, Opt. Mater. **62**, 651 (2016).

[16] See Supplemental Material at http://link.aps.org/supplemental/10.1103/PhysRevApplied.8.054002 for further information on structural properties and optical absorption edge of the grown thin films. Furthermore XPS measurements, which indicate tin is in a 4^+ oxidation state, are shown.

[17] Denis Machon, Paul F. McMillan, Bin Xu, and Jianjun Dong, High-pressure study of the β-to-α transition in ga_2o_3, Phys. Rev. B **73**, 094125 (2006).

[18] Simon Penner, Chen Zhuo, Ramona Thalinger, Matthias Grünbacher, Clivia Hejny, Stefan Vanicek, and Michael Noisternig, Physico-chemical properties of unusual Ga_2O_3 polymorphs, Monatsh. Chem. **147**, 289 (2016).

[19] D. Dohy, G. Lucazeau, and A. Revcolevschi, Raman spectra and valence force field of single-crystalline β-Ga_2O_3, J. Solid State Chem. **45**, 180 (1982).

[20] Yidong Hou, Ling Wu, Xinchen Wang, Zhengxin Ding, Zhaohui Li, and Xianzhi Fu, Photocatalytic performance of α-, β-, and γ-Ga_2O_3 for the destruction of volatile aromatic pollutants in air, J. Catal. **250**, 12 (2007).

[21] H. Seshadri, M. Cheralathan, and P. K. Sinha, Photocatalytic performance of combustion-synthesized β and γ-Ga_2O_3 in the degradation of 1,4-dioxane in aqueous solution, Research on chemical intermediates **39**, 991 (2013).

[22] D. R. Lide, *CRC Handbook of Chemistry and Physics* (CRC Press, Boca Raton, 2004).

[23] C. N. Cochran and L. M. Foster, Vapor pressure of gallium, stability of gallium suboxide vapor, and equilibria of some reactions producing gallium suboxide vapor, J. Electrochem. Soc. **109**, 144 (1962).

[24] J. B. Varley, J. R. Weber, A. Janotti, and C. G. Van de Walle, Oxygen vacancies and donor impurities in β-Ga_2O_3, Appl. Phys. Lett. **97**, 142106 (2010).